CrystEngComm

ROYAL SOCIETY OF CHEMISTRY

PAPER

View Article Online
View Journal | View Issue

Check for updates

Cite this: *CrystEngComm*, 2023, **25**, 3988

Forced topochemistry of a solid-state Diels–Alder reaction by encapsulation in epoxy glue†

T. A. Lau, S. Khorasani and M. A. Fernandes *

We report on the solid-state Diels–Alder thermal reaction in a 1 : 1 charge-transfer (CT) crystal composed of bis(*N*-cyclobutylimino)-1,4-dithiin (the electron acceptor) and 9-bromoanthracene (the electron donor) which crystallized in the triclinic space group, $P\bar{1}$. The donor (**D**) and acceptor (**A**) molecules arrange in stacks where these molecules alternate, where a full 9-bromoanthracene donor molecule is surrounded by a symmetrically different acceptor molecule on the two molecular faces. The distance between the reacting atoms on the donor and the two acceptor molecules are slightly different but still within Schmidt's criteria, resulting in two reaction sites with different reaction environments, assigned as regions **P** and **Q**. Molecules in region **P** are more favourably aligned with the distances between reacting atoms being 3.51 Å and almost parallel as the molecules overlap each other. In region **Q**, the distances are 3.56 and 3.86 Å because the molecular overlap is more skewed, and the reacting atoms are rotated −15° from each other. Initially, the reaction occurs only in region **P** until ∼20% conversion is reached. Afterward, product **Q** is concurrently formed but at a slower rate. After ∼75% reaction, the crystal transforms from triclinic $P\bar{1}$ into monoclinic $C2/c$, and conversion of ∼89% was found before the single crystal decomposes to become a powder. Reactions in free (unencapsulated) crystals above 10 °C were found to break apart during the initial reaction at around ∼20% when molecules in region **P** were reacting. Encapsulation of unreacted crystals with epoxy glue led to more reaction details being exposed and forced the reaction to occur topochemically until ∼89% conversion.

Received 19th April 2023,
Accepted 23rd May 2023

DOI: 10.1039/d3ce00388d

rsc.li/crystengcomm

Open Access Article. Published on 24 Thang Nm 2023. Downloaded on 17/05/2026 2:22:40 CH.
This article is licensed under a Creative Commons Attribution-NonCommercial 3.0 Unported Licence.

Introduction

Solid-state chemistry encompasses a vast array of reactions consisting of inorganic and organic materials.[1–6] Several studies suggest that solid-state reactions have been known to give higher yields of regio- and stereo-selective products than traditional solvent-based reactions, as well as using less solvents to make greener reactions.[7–12] Organic solid-state reactions can occur within single crystals and these can have many applications and consequences in various industries, such as in pharmaceuticals,[13–15] electronics,[16–18] and optics.[19–21] Single crystals that have undergone reactions in the solid state have been shown to occur under different conditions such as light,[7,22] heat[23–25] or pressure,[26–30] giving way to a variety of reactions with crystal products showing physical properties ranging from the formation of porous molecules[31–33] to mechanical effects.[34–36] These reactions fall in the domain of supramolecular chemistry, as intermolecular bonds between discrete molecules can lead to favourable conditions under which reactions can occur.[2] Topochemistry was first described by Kohlschütter as reactions that can occur in the solid state where the 3D nature of the crystal influences the structures and supramolecular arrangement of molecules in a crystal system, affecting the mechanism of the reaction.[7,9] To determine whether a topochemical reaction can occur in a crystal, Schmidt and coworkers' extensive work on [2 + 2] photodimerizations led to a topochemical criterion for solid-state reactions, where the reacting atoms need to be parallel to each other and within the distance of 3.5–4.2 Å.[37,38] Additionally, topochemical reactions occur best under minimal atomic movement, where the crystal integrity can be maintained. This is especially important when considering the reaction cavity of the reacting molecules, as the environment for which a reaction can occur in the solid-state is constrained by neighbouring molecules, influencing the product that can be formed.[39] The viability of a solid-state reaction in a crystal can be affected by adjacent molecules as they may hinder possible chemical products forming, even if

Molecular Sciences Institute, School of Chemistry, University of the Witwatersrand, PO Wits 2050, Johannesburg, South Africa. E-mail: Manuel.Fernandes@wits.ac.za; Fax: +27 11 7176749; Tel: +27 11 7176723

† Electronic supplementary information (ESI) available: Crystal coordinates as CIF files for all the structures reported in Table 1 have been deposited (Deposition Numbers 2257541–2257546) as a compressed file, as well as a PDF file containing supplementary information discussed in the text. For ESI and crystallographic data in CIF or other electronic format see DOI: **https://doi.org/10.1039/d3ce00388d**

This journal is © The Royal Society of Chemistry 2023

Open Access Article. Published on 24 Thang Nm 2023. Downloaded on 17/05/2026 2:22:40 CH.
This article is licensed under a Creative Commons Attribution-NonCommercial 3.0 Unported Licence.

Schmidt's criterion is met. An example of this is seen in work done by Botes *et al.*, where the cycloadduct product from the solid-state reaction of bis(*N*-benzylimino)-1,4-dithiin and various anthracene molecules could not be formed due to the reaction cavity not being flexible enough to allow for the movement of the reacting molecules, even while they meet Schmidt's criterion.[40] Reactions that proceed in a SCSC fashion occurs when the reactant crystal starts as a single crystal and ends with the product remaining as a single crystal whilst maintaining its shape and transparency.[41] This type of reaction is said to occur under topochemical control, where an SCSC reaction will start and continue in an SCSC manner until it is complete. However, if the final product crystal loses integrity during the reaction, it is said to be topotactic. In this case, the final product does not form a single crystal but shows an orientational relationship to the starting crystal.[42,43] Additionally, a SCSC product can form without sharing any crystallographic axes with the reactant crystal.[44]

In a previous paper,[23] we published the solid-state reaction of the charge transfer (CT) crystal of bis(*N*-cyclobutylimino)-1,4-dithiin (**A**, the charge acceptor molecule) and 9-bromoanthracene (**D**, the charge donor molecule) which formed dark red plate-like crystals in the space group $P\bar{1}$ (Scheme 1). The molecules arrange as stacks in a 2 : 1 **D** to **A** ratio for a ⋯{**D**⋯**A**⋯**D**}⋯{**D**⋯**A**⋯**D**}⋯{**D**⋯**A**⋯**D**}⋯ arrangement (Fig. 1). In terms of a thermal Diels–Alder reaction, a **D** molecule can only react with an **A** molecule to form a cycloadduct product (**P**). As such, the 2 : 1 **D** to **A** packing arrangement affects the solid-state reaction because an **A** molecule can react with the **D** molecule to the left or the right of it (or above and below it in Fig. 1) forming a cycloadduct product (**P**). A **D** molecule can only react with one **A** molecule because the neighbouring molecule in the stack is another **D** molecule which means that the molecules are constrained to a reaction site which we defined as a ⋯{**D**⋯**A**⋯**D**}⋯ unit. The **A** molecule can react with the **D** molecule to the left forming a product leading to this arrangement ⋯{**P**⋯**D**}⋯, or to the right of it leading to this arrangement ⋯{**D**⋯**P**}⋯. If cooperativity plays a role in the reaction, we can either have a sequence of products and unreacted **D** of ⋯{**D**⋯**P**}⋯{**D**⋯**P**}⋯{**D**⋯**P**}⋯ or ⋯**D**}⋯{**D**⋯**P**}⋯{**P**⋯**D**}⋯{**D**⋯ where the brackets represent the boundary of the **DAD** unit in the unreacted crystal (Fig. 1). If the reaction was random, we would not be able to find a sequence. However, our results indicated that the reaction was cooperative and led to a ⋯**D**}⋯{**D**⋯**P**}⋯{**P**⋯**D**}⋯{**D**⋯ arrangement. The reaction of the 2 : 1 CT underwent the solid-state Diels–Alder reaction through a topochemical SCSC mechanism, where the reaction cavity stayed relatively constant throughout the reaction and reached a 100% conversion with minimal crystal degradation.

During the previous study, we also found another CT co-crystal that crystallized in a 1 : 1 **D** to **A** forming a ⋯**D**⋯**A**⋯**D**⋯**A**⋯**D**⋯ arrangement within a brown needle-like crystal habit. Unlike the 2 : 1 CT, the solid-state reaction in the 1 : 1 CT leads to crystal fragmentation which happens around 20% conversion and therefore doesn't occur as an SCSC reaction without intervention. In this paper, we report on the solid-state reaction of this crystal.

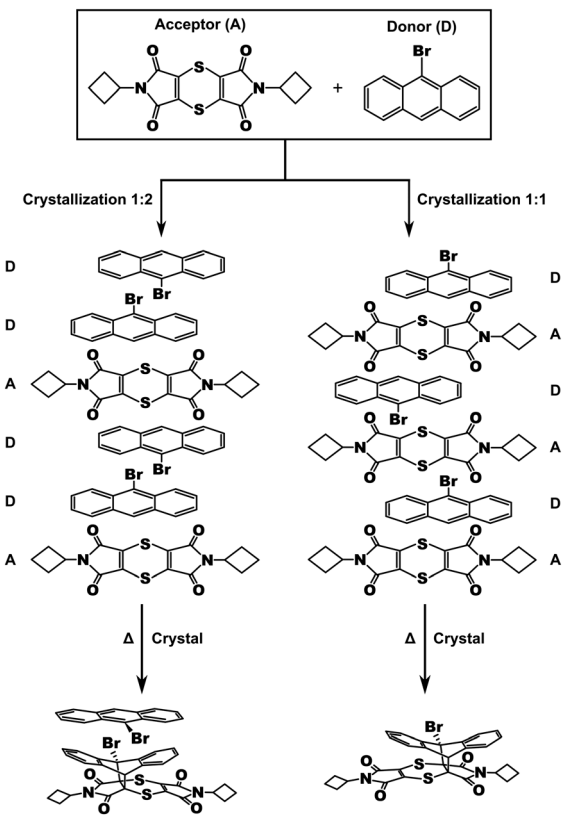

Scheme 1 Crystallization of bis(*N*-cyclobutylimino)-1,4-dithiin (**A**) and 9-bromoanthracene (**D**) leads to 1 : 2 **A** to **D** crystals (left),[23] and 1 : 1 **A** to **D** crystals (right, this work).

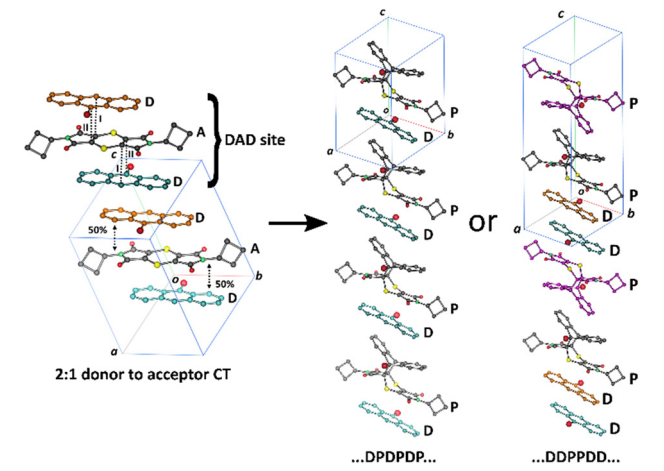

Fig. 1 Solid-state reaction in a 2 : 1 **D** to **A** CT co-crystal leading to two possible arrangements of product to donor arrangements if the reaction is cooperative. We found that SCSC reaction leads to the ⋯**D**⋯**D**⋯**P**⋯**P**⋯ arrangement shown on the right.[23]

Open Access Article. Published on 24 Thang Nm 2023. Downloaded on 17/05/2026 2:22:40 CH.
This article is licensed under a Creative Commons Attribution-NonCommercial 3.0 Unported Licence.

Materials and methods

Materials

Pure reagents were purchased from Sigma Aldrich and used as received. Solvents used in syntheses and recrystallization were purchased from Merck SA.

Synthesis

Bis(*N*-cyclobutylimino)-1,4-dithiin was synthesized similarly to a previously reported procedure.[23]

Crystallization and solid-state reaction

CT co-crystals were formed *via* vapour diffusion by dissolving a 1 : 1 ratio of bis(*N*-cyclobutylimino)-1,4-dithiin (10 mg, 28 μmol) and 9-bromoanthracene (7 mg, 28 μmol) separately in 1 mL dichloromethane. Upon addition of 9-bromoanthracene (**D**) into the bis(*N*-cyclobutylimino)-1,4-dithiin (**A**) vial, a change in colour occurred indicating CT formation. Vapour diffusion into hexane at 10 °C led the formation of brown needle shaped 1 : 1 **D** to **A** co-crystals. The co-crystals were reacted in a large capped test tube at either 20 °C (room temperature), or 40 °C using a water bath over various times and subsequently analyzed with SCXRD. Sunlight was avoided by locating the bath in a dark room. Initially, crystals were reacted unconstrained. These only remained intact until ~20% conversion. Later crystals were encapsulated with epoxy glue and were stable until ~89% conversion. When not reacted or measured by SCXRD, the crystals were stored in a freezer at −20 °C to inhibit the reaction.

Crystal structure solution and refinement

Intensity data were collected at −100.2 °C on either a Bruker Apex II CCD with graphite monochromated Mo Kα radiation (50 kV, 30 mA), or a Bruker D8 Venture Bio PHOTON III diffractometer with a Mo Kα IμS DIAMOND source (50 kV, 1.4 mA) or Cu Kα IμS DIAMOND source (50 kV, 1.2 mA). The collection methods involved ω and ϕ scans of width 0.5–1.5° with 1024 × 1024 (CCD) or 1536 × 1025 (PHOTON III) bit data frames. Crystal structures were solved by intrinsic phasing using *SHELXT*. Non-hydrogen atoms were first refined isotropically followed by anisotropic refinement by full-matrix least square calculations based on F^2. *SHELXL-2018* restraints such as SIMU, RIGU, SADI, and SAME were used during the refinements as required. Software used to obtain the structures were as follows: data collection: *APEX2*[45] and *APEX4*;[45] cell refinement and data reduction: *SAINT*;[46] empirical absorption corrections and scaling of data: *SADABS*;[45] space group determinations: *XPREP*;[45] programs used to solve and refine structures: *SHELXT*[47] and *SHELXL-2018*;[48] molecular graphics: *OLEX2*,[49] *SCHAKAL-99*,[50] and *CrystalExplorer-21.5*;[51,52] software used to prepare material for publication: *OLEX2* and *PLATON*.[53]

Crystallographic information for all structures can be found in Tables S1 and S2 in the ESI.† Crystallographic information for the CT crystals before, and at various stages of conversion, and for the recrystallized product can be found in Table 1. ORTEP diagrams for the CT asymmetric unit before reaction, after 60% conversion in triclinic, and after a phase change to the monoclinic form are shown in Fig. 3. The 9-bromoanthracene molecule is disordered with the major orientation having ~97% bromine occupancy and ~3% in 180° rotation minor orientation (not shown in Fig. 3). The reaction of minor conformation is undetectable, and probably only occurs when the crystal transforms from triclinic to monoclinic as mentioned later.

Calculations

Hirshfeld surfaces and molecule···molecule interaction energies (Fig. 4) between the donor (**D**) and two unique acceptor molecules (**AP** and **AQ**) were calculated using *Gaussian-09*[54] and *CrystalExplorer-21.5*[52] with *B3LYP/6-31G(d,p)*.

Results and discussion

Crystallization of bis(*N*-cyclobutylimino)-1,4-dithiin (**A**) and 9-bromoanthracene (**D**) leads to a 1 : 1 CT complex in the $P\bar{1}$ space group as dark red/brown needles. The asymmetric unit consists of a full **D** molecule and two half **A** molecules located on different inversion centres (Fig. 3a and 4a). The molecules overlap to form stacks in a ···**D**···**A**···**D**···**A**··· arrangement (Fig. 3 and 4a). Every **D** and **A** molecule can react with a molecule below or above it, forming a cycloadduct. The reaction can therefore be truly random because there is not a defined reaction site as in the 2 : 1 crystal which has the **DAD** unit. However, a random reaction assumes that the packing doesn't influence the reaction.

The two **A** molecules around the **D** molecule are within Schmidt's criterion (Fig. 5). The distances of the reacting atoms from the **AP** acceptor to the **D** are 3.505 (C1R···C17R) and 3.508 Å (C8R···C16R), while the **AQ** acceptor distances to the **D** are 3.570 (C1R···C24R) and 3.859 Å (C8R···C25R). This creates a region where the reaction easily leads to the **P** product, and a region where the reaction is more hindered because of slight misalignment of the reacting atoms as well as close contacts to neighbouring stacks, hindering movement to form the **Q** product (Fig. 4 and 5).

Generally, the reaction proceeds in the following steps (Fig. 4):

1. When the crystals are initially reacted, products are formed in the **P** product region until ~20% conversion is reached (Fig. 4b).

2. Upon further reaction, products are formed in the **Q** product region concurrently with the **P** product formation (Fig. 4c). **Q** product formation lags behind **P** product formation (Fig. 6).

3. Upon reaction past 65%, the crystal changes phase, transforming from the space group $P\bar{1}$ to the space group $C2/c$ (Fig. 4d).

Initially, we did the solid-state reactions with free (unencapsulated) crystals exposed to air at room temperature

 This journal is © The Royal Society of Chemistry 2023

Open Access Article. Published on 24 Thang Nm 2023. Downloaded on 17/05/2026 2:22:40 CH.
This article is licensed under a Creative Commons Attribution-NonCommercial 3.0 Unported Licence.

Table 1 Selected crystallographic and refinement data for various crystals. Full crystallographic data for the measured crystals can be found in Table S1 in the ESI†

Crystal	Free CT crystal	Glue encapsulated CT crystals	Glue encapsulated 12d 9 h reacted at 20 °C	Glue encapsulated 103d 4 h reacted at 20 °C	Glue encapsulated 133d 5 h reacted at 20 °C	Recrystallized product
Reaction time/days	0	0	12	103	133	—
Conversion/%	0	0	20	64	79	—
Formula weight	$C_{30}H_{23}BrN_2O_4S_2$	$C_{30}H_{23}BrN_2O_4S_2$	$C_{30}H_{23}BrN_2O_4S_2$	$C_{30}H_{23}BrN_2O_4S_2$	$C_{30}H_{23}BrN_2O_4S_2$	$C_{30}H_{23}BrN_2O_4S_2$
Crystal system	Triclinic	Triclinic	Triclinic	Triclinic	Monoclinic	Monoclinic
a/Å	11.5055(3)	11.5018(5)	11.4616(6)	11.5260(10)	20.1661(11)	9.6809(3)
b/Å	11.9465(3)	11.9360(5)	11.9174(6)	11.8060(11)	11.7540(11)	8.4899(3)
c/Å	11.9621(3)	11.9547(5)	11.9565(6)	12.2903(11)	14.9001(12)	31.9397(10)
α/°	63.4540(10)	63.4820(10)	64.094(2)	63.453(4)	—	—
β/°	78.3230(10)	78.390(2)	78.975(2)	78.220(4)	131.943(5)	96.4800(10)
γ/°	62.1540(10)	62.1500(10)	62.088(2)	61.190(3)	—	—
Unit cell volume/Å^3	1300.50(6)	1298.39(10)	1297.97(12)	1310.8(2)	2627.0(4)	2608.35(15)
Temperature/K	173(2)	173(2)	173(2)	173(2)	173(2)	173(2)
Space group	$P\bar{1}$	$P\bar{1}$	$P\bar{1}$	$P\bar{1}$	$C2/c$	$P2_1/n$
Density (Calc.)/g cm^{-3}	1.582	1.585	1.585	1.570	1.566	1.578
Z	2	2	2	2	4	4
Radiation type	MoKα	MoKα	MoKα	MoKα	MoKα	MoKα
Absorption coefficient, μ/mm^{-1}	1.783	1.786	1.786	1.769	1.765	1.778
Absorption correction	Multi-scan	Multi-scan	Multi-scan	Multi-scan	Multi-scan	Multi-scan
2θ range for data collection/°	3.806 to 56.734	5.502 to 56.928	3.788 to 56.64	3.704 to 49.998	4.402 to 49.986	4.966 to 56.594
No. of reflections measured	36 453	79 342	49 988	40 827	52 117	129 158
No. of independent reflections	6498	6432	6432	4609	2305	6469
R_{int}	0.0687	0.0325	0.0600	0.0681	0.1477	0.0575
Final R_1 ($I > 2\sigma(I)$)	0.0422	0.0387	0.0693	0.1331	0.1082	0.0305
Final w$R(F^2)$ ($I > 2\sigma(I)$)	0.1081	0.1104	0.1928	0.4123	0.2874	0.0754
Final R_1 (all data)	0.0687	0.0446	0.0816	0.1635	0.1315	0.0325
Final w$R(F^2)$ (all data)	0.1143	0.1143	0.2008	0.4426	0.3122	0.0766
Goodness of fit on F^2	0.963	1.114	1.115	1.913	1.122	1.053
CCDC number	2257541	2257542	2257543	2257544	2257545	2257546

Open Access Article. Published on 24 Thang Nm 2023. Downloaded on 17/05/2026 2:22:40 CH.
This article is licensed under a Creative Commons Attribution-NonCommercial 3.0 Unported Licence.

(20 °C). Under these conditions, we were only able to react the crystals up to ~20% because the crystals degrade very quickly starting from the surface and going into the bulk, giving poor diffraction patterns showing powder rings. Using this approach, we could only study the initial stages of the reaction and only confirm that the **P** product was forming. Subsequently, we encapsulated the unreacted crystals in epoxy glue and did the solid-state reactions using these epoxy-coated crystals at either room temperature or 40 °C.

Comparing the unit cell of the free crystals and the epoxy-coated crystals the unit cell parameters are consistent and not affected by the glue (Table 1). Reaction after 20% conversion was only possible with the crystals protected by glue, and the highest conversion we obtained was around ~89% (Fig. 6). The lack of data between 2500–3100 hours (around 25 days) in Fig. 6 was caused by unsteady electricity supply and electricity generator problems causing us to shut down the X-ray instruments for around three weeks. Reaction at 20 °C took about 200 days and gave us better data, but we also carried out the reaction at 40 °C which took 12 days and yielded similar results. The plots of lattice parameters *vs.* conversion for crystals reacted at both temperatures are overlapped on plots in Fig. S2 in the ESI.†

Initially, product **Q** formation is inhibited by the reacting atoms in the **AQ** and **D** molecules being twisted out of alignment, and close interactions from molecules in neighbouring stacks forcing the molecule to align in an unfavourable orientation. Drawing the Hirshfeld surface around the **AQ** acceptor that leads to product **Q** shows regions of close contact around the periphery of the

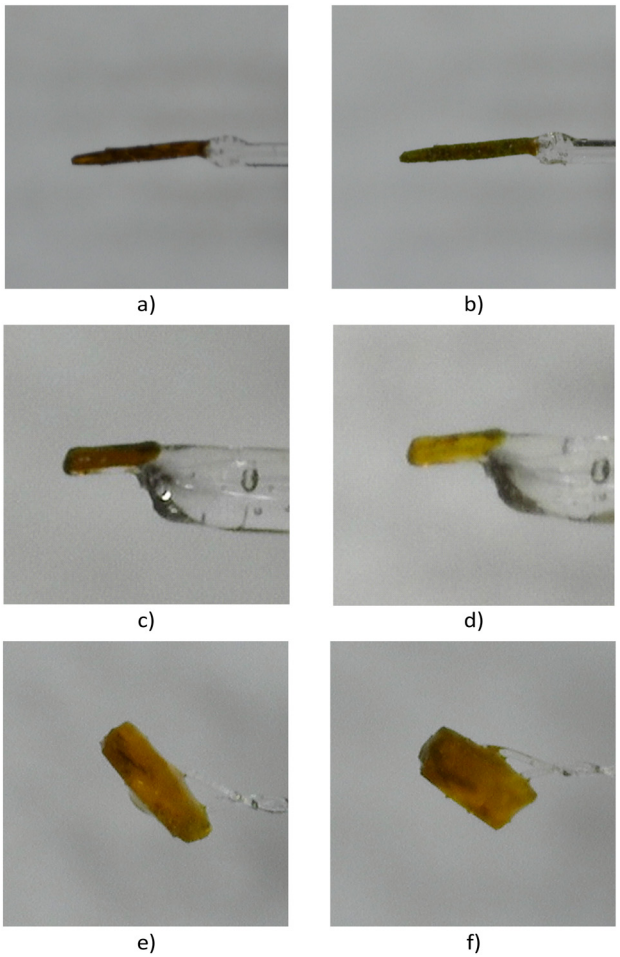

Fig. 2 Photographs of a crystal (0.10 × 0.10 × 0.86 mm) without glue before reaction (a) and after 4 days reaction at room temperature (b). The crystal decomposes to a powder at ~20% conversion. A crystal (0.08 × 0.09 × 0.29 mm) that was encapsulated with epoxy glue before reaction at room temperature (c) and reacted for 133 days (~79% conversion) at room temperature (d) was intact until ~89% conversion. Figures (e) and (f) are for a crystal (0.14 × 0.16 × 0.49 mm) without glue that was kept in a fridge at 10 °C for 2 years 77 days that reacted to ~87% conversion.

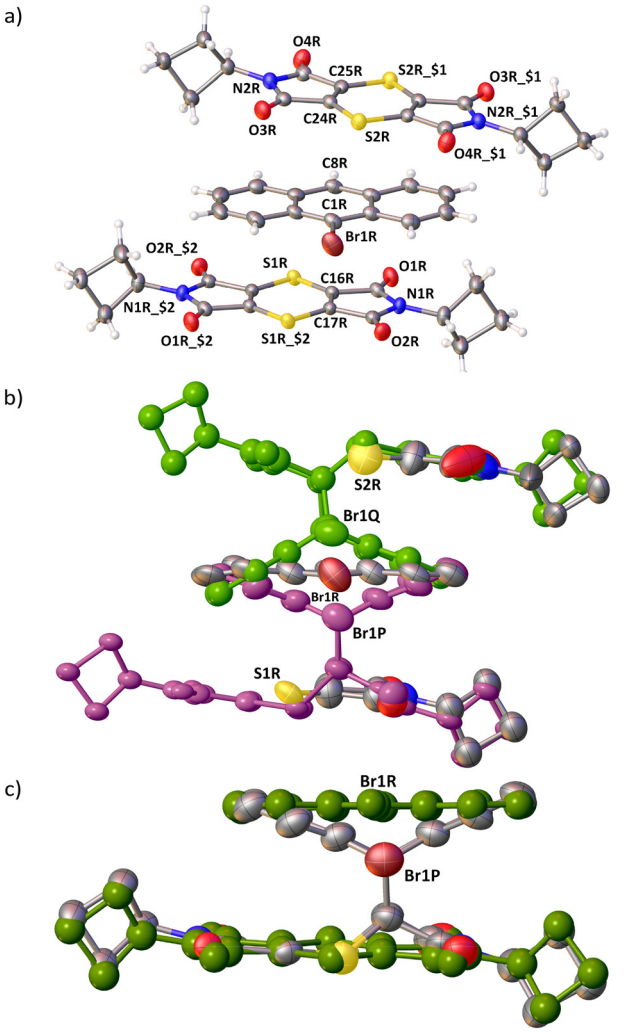

Fig. 3 ORTEP diagrams drawn at the 50% probability level. (a) The asymmetric unit of the 1:1 CT (initial) structure with hetero atoms labelled. Both the acceptor molecules are located on inversion centres ($1: 1 − *x*, 1 − *y*, 2 − *z*; $2: 2 − *x*, 1 − *y*, 1 − *z*). (b) The asymmetric unit showing the reactants and the **P** (purple) and **Q** (green) products at 70% conversion, just before the triclinic to monoclinic phase transition occurs. (c) The asymmetric unit in the monoclinic phase where more than 85% conversion has occurred. The remaining acceptor and donor are shown in green.

This journal is © The Royal Society of Chemistry 2023

Open Access Article. Published on 24 Thang Nm 2023. Downloaded on 17/05/2026 2:22:40 CH.
This article is licensed under a Creative Commons Attribution-NonCommercial 3.0 Unported Licence.

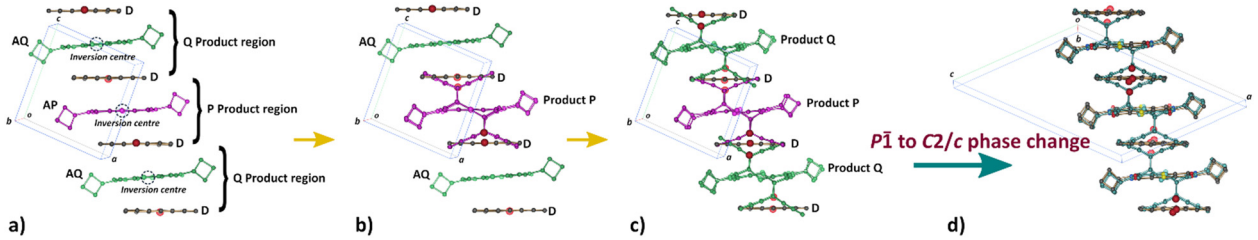

Fig. 4 Changes in unit cell contents because of the enforced SCSC Diels–Alder reaction. a) The initial CT crystal with a unique donor (**D**) and the acceptor in two different environments (**AP** and **AQ**; also see Fig. 5). Both acceptors are on a centre of inversion and reaction can occur with the donor above or below and appears to be disordered (product on both sides of the inversion). b) **AP** reacts to form product **P** and is the only product until ~20% conversion. c) Around 20% conversion, product **Q** is also formed alongside product **P**. d) When the crystal has reacted to more than 75%, a phase transformation from the initial triclinic space group $P\bar{1}$ to the monoclinic space group $C2/c$ occurs, in which the morphology of the stacks remains the same, but alignments between them have slightly changed.

molecule (Fig. 5). The Hirshfeld surface around the **AP** acceptor that leads to product **P** shows fewer regions with close contacts. Additionally, the **AP** acceptor atoms involved in the Diels–Alder reaction are aligned to react with the donor reacting atoms showing a torsion angle of 2.55°, while the **AQ** acceptor reacting atoms are not aligned as shown by the torsion angle of −15.33 °. The **AQ** acceptor would need to move into the optimal position for the Diels–Alder reaction to occur. Product **Q** formation is inhibited when conversion is lower than ~20% as the geometry is not ideal and lacks space for the **AQ** molecule to adjust to a favourable geometry. The space is created once product **P** has formed to a certain point, allowing for concurrent formation of product **P** and **Q**.

Around 75% conversion, the crystal undergoes a phase change from triclinic $P\bar{1}$ to monoclinic $C2/c$ with the unit cell doubling in volume (Table 1). The transformation matrix from the original triclinic to a monoclinic cell is (2−1 0)/(0−1 0)/(−1 1−1). This is not unprecedented because we have found, during a previous solid-state reaction study, that the crystal can lose symmetry and regain it again.[55] The unreacted CT crystallized in the space group $P2_1/n$, and during the initial reaction the crystal refined in $P2_1/n$ with R-factor (R_1) below 10% when the conversion was below 28%, but rapidly shot up to ~19% when the conversion was between 28–80%. Refining the crystal when the conversion was between 28–80% in $P2_1$ resulted in the R_1 value being lower than the $P2_1/n$ values by 5%. After 80% conversion the refinements in $P2_1$ and $P2_1/n$ resulted in similar R_1 values of around 9%. During conversion between 28–80%, n-glide symmetry in the crystal was lost which was why refining the crystal in $P2_1/n$ led to high R_1 values, but it was later regained after 80% while the crystal was adjusting to the solid-state product.

Initially, the solid-state reaction depends on the alignment of the reactants and the packing of the CT structure which will influence the site and direction of the product formation. However, once the product dominates the crystal, it influences the crystal structure of the final reacted crystal. In the previous studies, the crystal started in the space group $P2_1/n$ and remained in this space group at the end. In this work, the reacting crystal transformed from a lower symmetry space group ($P\bar{1}$) to a higher symmetry space group ($C2/c$), acquiring a c-glide plane and a 2-fold axis, and retaining the inversion centres (Fig. 7). The transformation from $P\bar{1}$ to $C2/c$ is not perfect and the reacting crystal probably goes through intermediate space groups on the way. For the space group $C2/c$, the c-glide perpendicular to the b-axis will lead to the systematic absence of the ($h0l$) family of reflections which

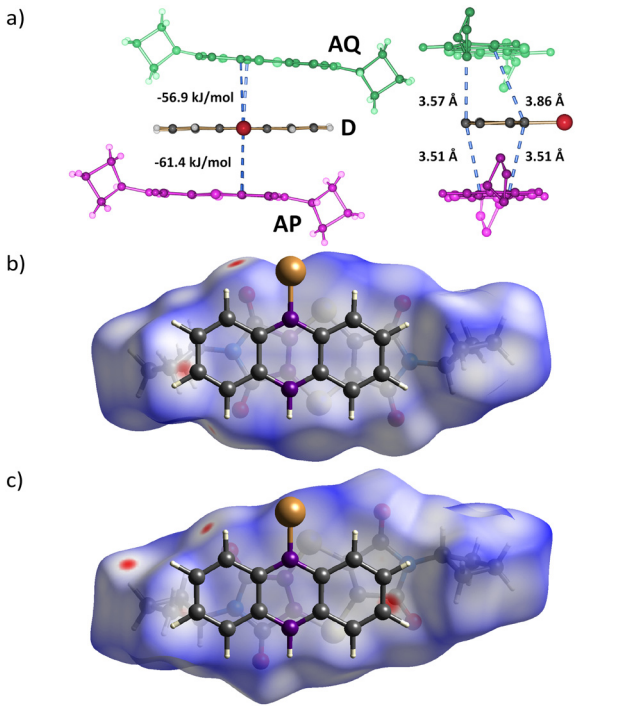

Fig. 5 The reaction environment between the **AP** and **AQ** acceptor and **D** molecules. (a) The distance between the reacting atoms in the **AP** and **D** molecules to form the product **P** is around 3.51 Å and are almost parallel as shown in (b). The distances between the reacting atoms in the **AQ** and **D** molecules to form product **Q** are very unequal because the molecular overlap is offset. The molecules are rotated slightly, and the red spots on the edges of the Hirshfeld surface show interactions with neighbouring stacks (c). However, the interaction energy between **AP** and **AQ** and the **D** molecule at −61.4 and −56.9 kJ mol^{-1}, respectively, do not differ that much.

Open Access Article. Published on 24 Thang Nm 2023. Downloaded on 17/05/2026 2:22:40 CH.
This article is licensed under a Creative Commons Attribution-NonCommercial 3.0 Unported Licence.

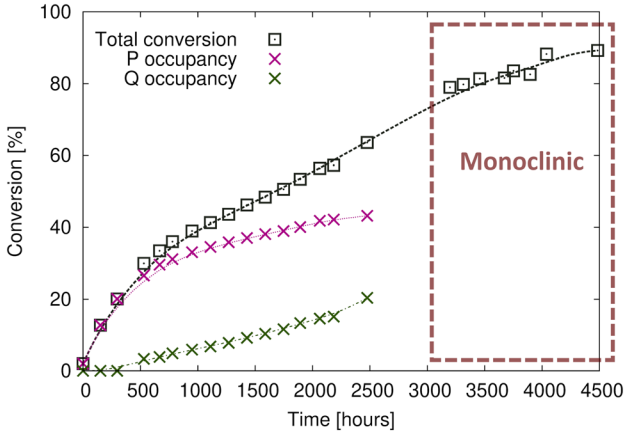

Fig. 6 Product formation at 20 °C with crystals encapsulated by glue. Product **P** is formed initially until ~20% conversion. Afterward, product **Q** is concurrently formed but at a slower rate. After, 2500 hours of reaction (~75% conversion) a phase change occurs from triclinic $P\bar{1}$ to monoclinic $C2/c$, where the occupancies of products **P** and **Q** are about the same because the space group $C2/c$ is centrosymmetric, and the structure refines with one unique product molecule in the asymmetric unit.

will be absent when $l \neq 2n$. When solving the structure of the reacted crystals after the transition from triclinic to monoclinic, there are many *c*-glide systematic absence violations, but the structures refine acceptably. However, with increasing percent conversion, the *c*-glide systematic absence violations decrease.

Pseudo ($h0l$) precession images calculated from single-crystal X-ray diffraction data for the triclinic structure reacted crystal at 64% conversion (Table 1) just before transformation, after $P\bar{1}$ to $C2/c$ transformation at 79% (Table 1) and 89% (Table S1 in the ESI†) are shown in Fig. 8. The triclinic structure was transformed to monoclinic using the (2−1 0)/(0−1 0)/(−1 1−1) transformation matrix from the triclinic cell. The transformation of a 64% reacted crystal generates a cell (a = 20.217 Å, b = 11.806 Å, c = 14.857, α = 92.93°, β = 132.15°, γ = 88.03°) which is very close to the monoclinic cell of the 79% reacted crystal (a = 20.166 Å, b = 11.754 Å, c = 14.900, α = 90°, β = 131.94°, γ = 90°). In the ($h0l$) precession images, the triclinic cell shows the expected $h0l$: $l \neq 2n$ violations, but these become less after transformation to monoclinic at ~79% conversion and are absent at ~89% conversion (Fig. 8 and S1 in the ESI†). With more conversion the reacted crystal conforms more closely to $C2/c$ as the crystal adapts to the product.

To compare the unit cell changes occurring due to the solid-state reaction on the same graphs, the monoclinic unit cells were transformed to the triclinic unit cell of the CT using ($\frac{1}{2}$ $\frac{1}{2}$ 0)/(0−1 0)/(−$\frac{1}{2}$ −$\frac{1}{2}$ −1). These points are highlighted in Fig. 9 and the crystallographic information can be found in Tables 1 and S2 in the ESI.†

During the reaction, the *a*- and *c*-axes expand by around 6% and 2% respectively, while the *b*-axis contracts by around 1% (Fig. 9a). It is interesting that the trend line for the reacting crystal follows a smooth path that coincides with the

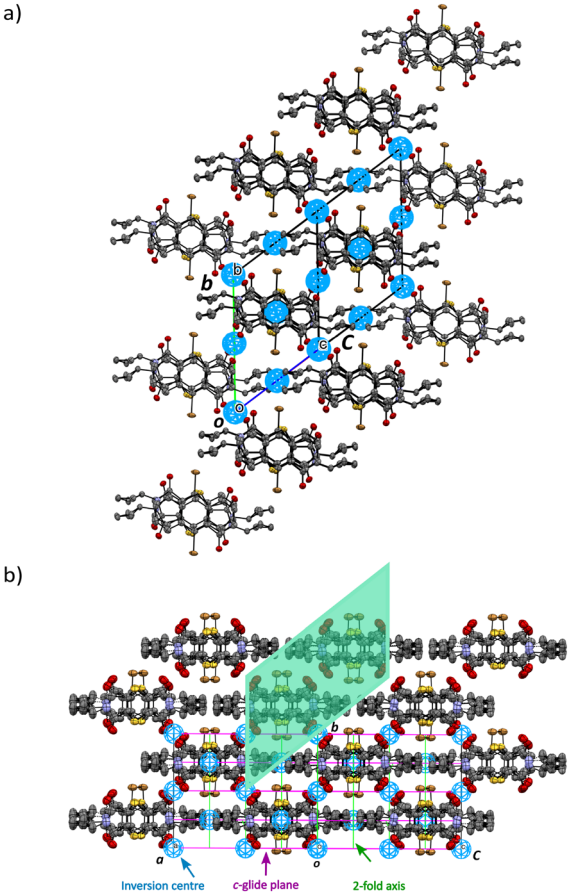

Fig. 7 Unit cell and symmetry changes on transforming from the space group $P\bar{1}$ triclinic CT before reaction (a), to the final solid-state reacted crystal in the space group $C2/c$ monoclinic form (b). In the monoclinic form, the **P** and **Q** products are in equal amounts because they are related by a centre of inversion in $C2/c$. In the triclinic form (a), occupancy of the products just before the transformation is around 40% for **P** and 20% for **Q** (Fig. 6).

converted monoclinic points for all axes, implying that the crystal does not suddenly transform into the monoclinic form after a certain amount of reaction has occurred, but gradually transforms with conversion to the monoclinic form. Smooth trend lines can also be seen when looking at the cell angles for the reacting crystal (Fig. 9b). In this case, the α- and β-angles decrease by around 2%, while the γ-angle decreases by around 4%. The cell volume increases by 3.5% which is consistent with the increasing disorder of the reacting crystal.

A reviewer pointed out that the SCXRD data was collected at −100 °C and there was a possibility that $P\bar{1}$ to $C2/c$ transformation could occur upon cooling the crystals to this temperature. This is unlikely because changes in unit cell parameters with conversion shown in Fig. 9 are very gradual and linked to percent conversion. However, to make sure a crystal (Fig. 2) stored in a fridge set at 10 °C from the start of the project (2 years and 77 days ago from the date recorded on the vial) was selected and room temperature SCXRD data set was collected before measuring a data set at −100 °C.

 This journal is © The Royal Society of Chemistry 2023

Open Access Article. Published on 24 Thang Nm 2023. Downloaded on 17/05/2026 2:22:40 CH.
This article is licensed under a Creative Commons Attribution-NonCommercial 3.0 Unported Licence.

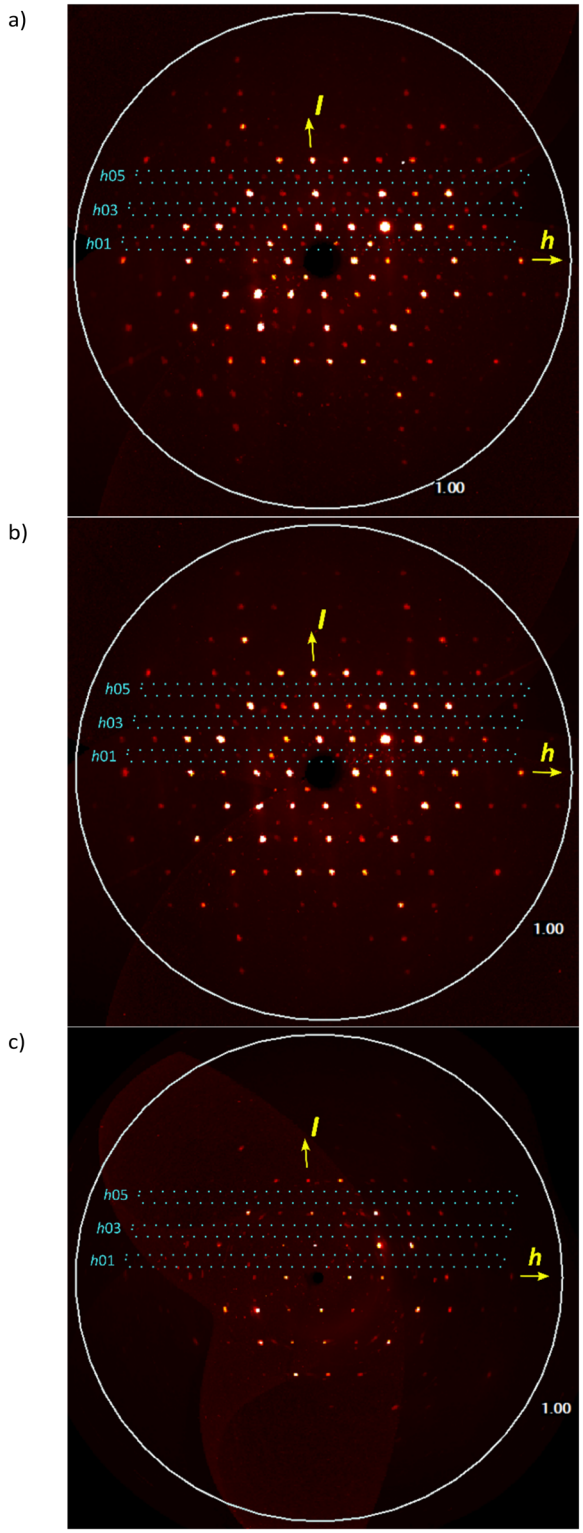

Fig. 8 Pseudo (*h*0*l*) precession images for (a) the room temperature reacted crystal at ~64% (just before transformation), and after the $P\bar{1}$ to *C*2/*c* transformation at (b) ~79% and (c) ~89% conversion. The (*h*01), (*h*03), and (*h*05) reflections enclosed with dotted lines are allowed in the triclinic $P\bar{1}$ space group (a) but are weaker in (b) and absent in (c) as required for *C*2/*c*.

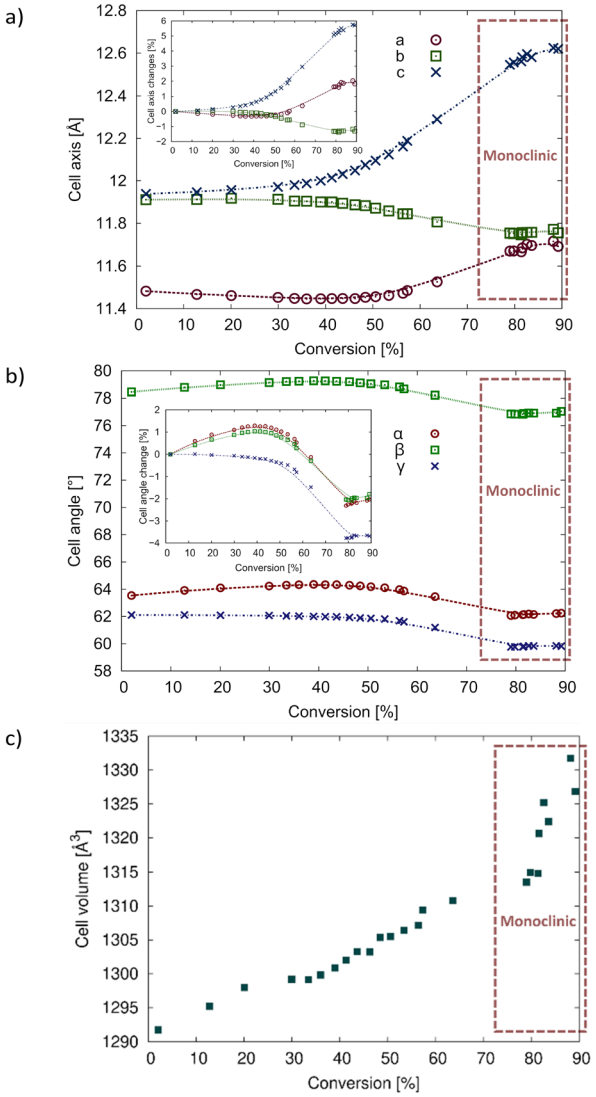

Fig. 9 Changes in unit cell parameters with degree of conversion for the crystal reacted at 20 °C. The points that are enclosed with a red rectangle were transformed from the monoclinic unit cell back to the triclinic cell of the CT (see text for details). (a) Changes in *a*–*c* with the inset graph showing the percent change; (b) change in cell angles with the inset graph showing the percent change; (c) change in cell volume. Plots of the 40 °C data are superimposed on this data in Fig. S2 in the ESI.†

Both crystal structures solved in the space group *C*2/*c* (Table S3 in the ESI†) indicating that no temperature-dependent phase change occurs. The unit cell parameter at −100 °C for this structure is plotted with the RT and 40 °C data in Fig. S2 in the ESI† and coincides with these data.

Finally, the product was recrystallized to compare the unit cell, space group, and crystal packing with the solid-state reaction monoclinic form. It crystallizes in the monoclinic space group $P2_1/n$ in a different unit cell (Table 1 and Fig. 10). The crystal packing is also different. While the solid-state reaction product molecules are arranged as stacks due to the templating effect of the starting CT coordinates (Fig. 4d), the molecules in the recrystallized structure are packed to optimize hydrogen bonding and other interactions,

Open Access Article. Published on 24 Thang Nm 2023. Downloaded on 17/05/2026 2:22:40 CH.
This article is licensed under a Creative Commons Attribution-NonCommercial 3.0 Unported Licence.

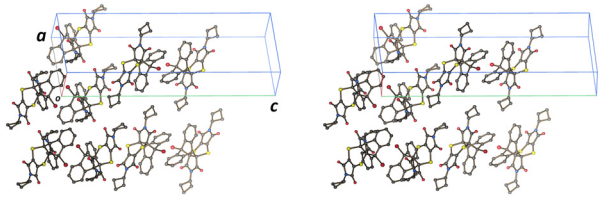

Fig. 10 Stereo diagram of the crystal packing of the recrystallized Diels–Alder product.

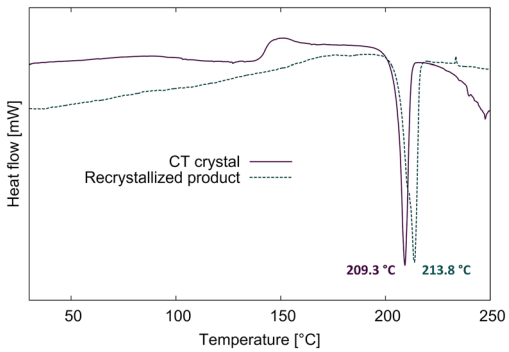

Fig. 11 DSC scans for a fresh CT crystal and a recrystallized crystal until their melting point. The CT crystal shows a reaction between 100–150 °C, and the melting peak is 4.5 °C lower than the recrystallized crystal.

with the molecules arranged side-to-side favouring H-bonding, head-to-head favouring π···π interactions, or forming T-shaped arrangements favouring C═O···π interactions (Fig. 10). Due to the optimized hydrogen bonding and other interactions, the recrystallized structure will be more stable than the metastable solid-state reaction derivative which is why it undergoes a phase transformation during the later stages of reaction.

The DSCs of the CT and the recrystallized product are shown in Fig. 11. When a fresh CT crystal is heated in the DSC at 10° min^{-1} under nitrogen, it reacts between 100–150 °C (possibly with a recrystallization phase at ~150 °C) then melts at 209.3 °C. The recrystallized product melts at 213.8 °C which is 4.5 °C higher than the solid-state reacted CT crystal. We also did a DSC of a CT crystal in which the crystal was heated until 180 °C to avoid melting. When we opened the aluminium pan afterward, we found a yellow single crystal which the SCXRD analysis revealed was the same crystal structure as the recrystallized product. The lower melting point of the DSC reacted CT is probably because the solid-state reaction doesn't lead to a pure product, and not because it is a new polymorph. We also found that the final crystal structure for one experiment was that of the recrystallized structure which self-assembled and annealed as a single crystal in the epoxy glue towards the end of the reaction process. Therefore, the space group for the reacted crystal transitions from $P\bar{1}$ to the metastable form $C2/c$, which then recrystallizes in the solid state to the thermodynamically stable $P2_1/n$.

Conclusions

Crystallizing 9Br and DiC4 as a 1 : 1 CT leads to a triclinic $P\bar{1}$ crystal in which the **D** and **A** molecules form stacks in a ···**D**···**A**···**D**···**A**··· arrangement. Two half acceptor molecules sit on different inversion centres, together with a full donor molecule. The environments of these two acceptors guide the behaviours in the reaction. The more favourable aligned acceptor leads to the initial formation of product **P** exclusively until ~20% conversion, then the second acceptor also reacts to form product **Q**. The reacting crystal remains in triclinic space group $P\bar{1}$ until ~65% conversion has occurred, then transforms to monoclinic space group $C2/c$, which is probably a type II phase transformation that occurs during the reaction. Transforming the monoclinic structures into the triclinic phase using the transformation matrix $(\frac{1}{2}\ \frac{1}{2}\ 0)/(0\ {-1}\ 0)/(\frac{-1}{2}\ \frac{1}{2}\ {-1})$ to plot all the cell parameters on the same graph with percent conversion, it is evident that phase transformation doesn't occur instantly, but as a gradual process. The product crystal in space group $C2/c$ is accessible by doing the solid-state reaction using a crystal encapsulated in epoxy glue. It is also possible to study the reaction without epoxy encapsulation at 10 °C or lower, but in such conditions, the reaction would take an extended period of time, possibly years. As an alternative experimental method, moderate to high pressures using a diamond anvil cell can also force this reaction to occur topochemically and with alternative reaction paths and greater yield depending on the pressure used.[26–30]

Conflicts of interest

There are no conflicts to declare.

Acknowledgements

The authors wish to thank the University of the Witwatersrand as well as the South African National Research Foundation (CPRR 111705; GUN 77122 and 110539) for financial support.

References

1 A. R. West, *Solid State Chemistry and its Applications*, John Wiley & Sons, Ltd, Kilbride, 1992.
2 L. R. Macgillivray, G. S. Papaefstathiou, T. Friščić, T. D. Hamilton, D. K. Bučar, Q. Chu, D. B. Varshney and I. G. Georgiev, *Acc. Chem. Res.*, 2008, **41**, 280–291.
3 E. A. Moore and L. E. Smart, *Solid State Chemistry: An Introduction*, CRC Press, Oxfordshire, 5th edn, 2021.
4 R. E. Schaak and T. E. Mallouk, *Chem. Mater.*, 2002, **14**, 1455–1471.
5 H. Schmalzried and M. Backhaus-Ricoult, *Prog. Solid State Chem.*, 1993, **22**, 1–57.
6 Z. 'A. Mohiju, M. Mujaini and N. A. Hamid, *IOP Conf. Ser.: Mater. Sci. Eng.*, 2022, **1231**, 012009.
7 V. Ramamurthy and K. Venkatesan, *Chem. Rev.*, 1987, **87**, 433–481.

 This journal is © The Royal Society of Chemistry 2023

Open Access Article. Published on 24 Thang Nm 2023. Downloaded on 17/05/2026 2:22:40 CH.
This article is licensed under a Creative Commons Attribution-NonCommercial 3.0 Unported Licence.

8 K. Biradha and R. Santra, *Chem. Soc. Rev.*, 2013, **42**, 950–967.
9 K. Hema, A. Ravi, C. Raju, J. R. Pathan, R. Rai and K. M. Sureshan, *Chem. Soc. Rev.*, 2021, **50**, 4062–4099.
10 F. Toda, *Acc. Chem. Res.*, 1995, **28**, 480–486.
11 G. Kaupp, *Top. Curr. Chem.*, 2005, **254**, 95–183.
12 D. Braga, D. D'Addario, S. L. Giaffreda, L. Maini, M. Polito and F. Grepioni, *Top. Curr. Chem.*, 2005, **254**, 71–94.
13 R. Breinbauer, I. R. Vetter and H. Waldmann, *Angew. Chem., Int. Ed.*, 2002, **41**, 2878–2890.
14 S. R. Byrn, R. R. Pfeiffer, G. Stephenson, D. J. W. Grant and W. B. Gleason, *Chem. Mater.*, 1994, **6**, 1148–1158.
15 *Polymorphism in the Pharmaceutical Industry: Solid Form and Drug Development*, ed. R. Hilfiker and M. von Raumer, Wiley-VCH Verlag GmbH, Weinheim, 2nd edn, 2019.
16 K. P. Goetz, D. Vermeulen, M. E. Payne, C. Kloc, L. E. McNeil and O. D. Jurchescu, *J. Mater. Chem. C*, 2014, **2**, 3065–3076.
17 T. Wang, X. Su, X. Zhang, X. Nie, L. Huang, X. Zhang, X. Sun, Y. Luo, G. Zhang, T. Wang, X. Zhang, X. Nie, L. Huang, Y. Luo, G. Zhang, X. Su and X. Sun, *Adv. Mater.*, 2019, **31**, 1904273.
18 Y. Jiang, Y.-Y. Liu, X. Liu, H. Lin, K. Gao, W.-Y. Lai and W. Huang, *Chem. Soc. Rev.*, 2020, **49**, 5885–5944.
19 M. Irie, S. Kobatake and M. Horichi, *Science*, 2001, **291**, 1769–1772.
20 H.-H. Fang, J. Yang, J. Feng, T. Yamao, S. Hotta and H.-B. Sun, *Laser Photonics Rev.*, 2014, **8**, 687–715.
21 A. Nitti and D. Pasini, *Adv. Mater.*, 2020, **32**, 1908021.
22 E. Heller and G. M. J. Schmidt, *Isr. J. Chem.*, 1971, **9**, 449–462.
23 S. Khorasani and M. A. Fernandes, *Chem. Commun.*, 2017, **53**, 4969–4972.
24 A. Pathigoolla and K. M. Sureshan, *Angew. Chem.*, 2013, **125**, 8833–8837.
25 D. S. Botes, S. Khorasani, D. C. Levendis and M. A. Fernandes, *CrystEngComm*, 2022, **24**, 7563–7569.
26 H. Jin, A. M. Plonka, J. B. Parise and N. S. Goroff, *CrystEngComm*, 2013, **15**, 3106–3110.
27 A. Friedrich, I. E. Collings, K. F. Dziubek, S. Fanetti, K. Radacki, J. Ruiz-Fuertes, J. Pellicer-Porres, M. Hanfland, D. Sieh, R. Bini, S. J. Clark and T. B. Marder, *J. Am. Chem. Soc.*, 2020, **142**, 18907–18923.
28 H. Chen, B.-B. Ni, F. Gao and Y. Ma, *Green Chem.*, 2012, **14**, 2703–2705.
29 J. Bąkowicz and I. Turowska-Tyrk, *CrystEngComm*, 2014, **16**, 6039–6048.
30 A. Delori, I. B. Hutchison, C. L. Bull, N. P. Funnell, A. J. Urquhart and I. D. H. Oswald, *Cryst. Growth Des.*, 2018, **18**, 1425–1431.
31 V. Guillerm, D. Kim, J. F. Eubank, R. Luebke, X. Liu, K. Adil, M. S. Lah and M. Eddaoudi, *Chem. Soc. Rev.*, 2014, **43**, 6141–6172.
32 I. E. Claassens, L. J. Barbour and D. A. Haynes, *J. Am. Chem. Soc.*, 2019, **141**, 11425–11429.
33 S. Horike, S. Shimomura and S. Kitagawa, *Nat. Chem.*, 2009, **1**, 695–704.
34 D. Hean, L. G. Alde and M. O. Wolf, *J. Mater. Chem. C*, 2021, **9**, 6789–6795.
35 P. Naumov, S. Chizhik, M. K. Panda, N. K. Nath and E. Boldyreva, *Chem. Rev.*, 2015, **115**, 12440–12490.
36 X. Ding, E. Zahid, D. K. Unruh and K. M. Hutchins, *IUCrJ*, 2022, **9**, 31–42.
37 G. M. J. Schmidt, *Pure Appl. Chem.*, 1971, **27**, 647–678.
38 M. D. Cohen and G. M. J. Schmidt, *J. Chem. Soc.*, 1964, 1996–2000.
39 E. V. Boldyreva, *Solid State Ionics*, 1997, **101–103**, 843–849.
40 D. S. Botes, S. Khorasani, W. Duminy, D. C. Levendis and M. A. Fernandes, *Cryst. Growth Des.*, 2020, **20**, 291–299.
41 T. Friščić and L. R. MacGillivray, *Z. Kristallogr. - Cryst. Mater.*, 2005, **220**, 351–363.
42 H. Morawetz, S. Z. Jakabhazy, J. B. Lando and J. Shafer, *Proc. Natl. Acad. Sci. U. S. A.*, 1963, **49**, 789–793.
43 G. Wegner, *Pure Appl. Chem.*, 1977, **49**, 443–454.
44 I. Halasz, *Cryst. Growth Des.*, 2010, **10**, 2817–2823.
45 *APEX2, Version 2.01 or APEX4, Version 2.01 (includes XPREP version 2014/2 and SADABS version 2016/2)*, Bruker AXS Inc., Madison, Wisconsin, USA, 2012.
46 *SAINT V8.34A or V8.40B*, Bruker AXS Inc., Madison, Wisconsin, USA, 2012.
47 G. M. Sheldrick, *Acta Crystallogr., Sect. A: Found. Adv.*, 2015, **71**, 3–8.
48 G. M. Sheldrick, *Acta Crystallogr., Sect. C: Struct. Chem.*, 2015, **71**, 3–8.
49 O. V. Dolomanov, L. J. Bourhis, R. J. Gildea, J. A. K. Howard and H. Puschmann, *J. Appl. Crystallogr.*, 2009, **42**, 339–341.
50 E. Keller, *SCHAKAL-99*, University of Freiberg, Germany, 1999.
51 M. A. Spackman and D. Jayatilaka, *CrystEngComm*, 2009, **11**, 19–32.
52 P. R. Spackman, M. J. Turner, J. J. McKinnon, S. K. Wolff, D. J. Grimwood, D. Jayatilaka and M. A. Spackman, *J. Appl. Crystallogr.*, 2021, **54**, 1006–1011.
53 A. L. Spek, *Acta Crystallogr., Sect. D: Biol. Crystallogr.*, 2009, **65**, 148–155.
54 M. J. Frisch, G. W. Trucks, H. B. Schlegel, G. E. Scuseria, M. A. Robb, J. R. Cheeseman, G. Scalmani, V. Barone, B. Mennucci, G. A. Petersson, H. Nakatsuji, M. Caricato, X. Li, H. P. Hratchian, A. F. Izmaylov, J. Bloino, G. Zheng, J. L. Sonnenberg, M. Hada, M. Ehara, K. Toyota, R. Fukuda, J. Hasegawa, M. Ishida, T. Nakajima, Y. Honda, O. Kitao, H. Nakai, T. Vreven, J. J. A. Montgomery, J. E. Peralta, F. Ogliaro, M. Bearpark, J. J. Heyd, E. Brothers, K. N. Kudin, V. N. Staroverov, R. Kobayashi, J. Normand, K. Raghavachari, A. Rendell, J. C. Burant, S. S. Iyengar, J. Tomasi, M. Cossi, N. Rega, N. J. Millam, M. Klene, J. E. Knox, J. B. Cross, V. Bakken, C. Adamo, J. Jaramillo, R. Gomperts, R. E. Stratmann, O. Yazyev, A. J. Austin, R. Cammi, C. Pomelli, J. W. Ochterski, R. L. Martin, K. Morokuma, V. G. Zakrzewski, G. A. Voth, P. Salvador, J. J. Dannenberg, S. Dapprich, A. D. Daniels, Ö. Farkas, J. B. Foresman, J. V. Ortiz, J. Cioslowski and D. J. Fox, *Gaussian-09, Revision E.01*, Gaussian Inc., Wallingford, CT, 2009.
55 S. Khorasani, D. S. Botes, M. A. Fernandes and D. C. Levendis, *CrystEngComm*, 2015, **17**, 8933–8945.